AGU PUBLICATIONS

Geochemistry, Geophysics, Geosystems

RESEARCH ARTICLE
10.1002/2016GC006602

Dynamics of primary productivity in the northern South China Sea over the past 24,000 years

Hongrui Zhang[1], Chuanlian Liu[1], Xiaobo Jin[1], Jiangnan Shi[1], Shaohua Zhao[1], and Zhimin Jian[1]

[1]State Key Laboratory of Marine Geology, Tongji University, Shanghai, China

Key Points:
- Quantitative reconstruction of primary productivity in the northern South China Sea
- Organic carbon burial efficiency may decrease from glacial to interglacial in the norther SCS
- The main controlling factor of primary productivity shifted from winter monsoon to El Niño

Supporting Information:
- Supporting Information S1

Correspondence to:
C. Liu,
liucl@tongji.edu.cn

Citation:
Zhang, H., C. Liu, X. Jin, J. Shi, S. Zhao, and Z. Jian (2016), Dynamics of primary productivity in the northern South China Sea over the past 24,000 years, *Geochem. Geophys. Geosyst.*, *17*, 4878–4891, doi:10.1002/2016GC006602.

Received 22 AUG 2016
Accepted 15 NOV 2016
Accepted article online 18 NOV 2016
Published online 17 DEC 2016

Abstract In this study, paleoproductivity on millennial scales was precisely reconstructed from core MD12-3428cq in the northern South China Sea (SCS) over the past 24 kyr, based on a transfer function derived from the strong exponential negative correlation between relative abundance of *Florisphaera profunda* (%FP) in core top sediments and basin-wide satellite-based primary productivity (PP) in the SCS. To detect the potential driving mechanisms of PP, correlation analyses were carried out among our PP records and other paleoenvironment parameters. PP peaked during 18–15 ka in parallel with the strong East Asian Winter Monsoon (EAWM). From 15 ka to the early Holocene, a decrease in PP coincided with sea level progradation and weakening of EAWM, which ultimately reduced fluvial nutrient levels and wind-driven upper water column mixing. Since the middle Holocene, gradually more frequent El Niño-Southern Oscillation (ENSO) events have taken place, further decreasing PP by injecting oligotrophic Kuroshio water masses into the northern SCS. Associated findings conclusively indicated that the main controlling factors of PP in the northern SCS have shifted from EAWM (glacial) to ENSO (interglacial) over the past 24 kyr.

1. Introduction

Phytoplankton is an important component in the global carbon cycle and variations in primary productivity (PP) are closely related to glacial-interglacial atmospheric CO_2 changes [*Martin*, 1990]. Coccolithophores are known as some of the most important primary producers in photic ocean layers. They can produce calcareous plates called coccoliths and essentially record paleoenvironmental details [e.g., *Giraudeau and Beaufort*, 2007]. Coccolithophores compose 10%–20% of the total chlorophyll-*a* (Chl-*a*) and phytoplankton carbon in the water columns under nonbloom conditions [*Poulton et al*., 2010], and coccolith-based calcite contributes to the majority of discrete particulate inorganic carbon and $CaCO_3$ fluxes [e.g., *Sprengel et al*., 2002; *Young and Ziveri*, 2000; *Jin et al*., 2016]. *Florisphaera profunda* is a lower photic dweller whose relative abundance has been widely used in paleoceanography studies as a reliable proxy for marine productivity and nutricline depth [e.g., *Molfino and McIntyre*, 1990; *Beaufort et al*., 1997, 2001], as well as in the South China Sea (SCS) [*Liu et al*., 2008; *Su et al*., 2013]. However, the numerical relationship between the percentage of *F. profunda* and annual PP presently remains unclear for the SCS.

Many proxies have been used in the SCS to reconstruct the paleoproductivity, such as organic carbon [e.g., *Huang et al*., 1997; *Löwemark et al*., 2009], biomarkers [e.g., *Higginson et al*., 2003; *Zhao et al*., 2006], biogenic opal [e.g., *Lin et al*., 1999; *Wang et al*., 2007], elements ratios [e.g., *Lin et al*., 1999; *Wei et al*., 2003], and nannofossil/microfossil assemblages [e.g., *Jian et al*., 2001; *Su et al*., 2013]. Previous studies have suggested that productivity was controlled by East Asian Winter Monsoon (EAWM) on orbital time scales in the northern SCS [e.g., *Higginson et al*., 2003; *He et al*., 2013], while the variation of productivity were heterogeneous in the rest of the SCS [e.g., *Wei et al*., 2003; *Wang et al*., 2007]. However, paleoproductivity variations on millennial scales are unclear and quantitative reconstructions of PP are limited compared with the great number of qualitative studies. In addition, modern observations suggest that El Niño can play important part in the variations of PP [e.g., *Liu et al*., 2002], while few studies focused on how the El Niño impacted the paleoproductivty in the SCS. Understanding PP dynamics of the past is important for interpreting the carbon cycle's response to climate change. Hence, in this study, analyses of the relative abundances of *F. profunda* (%FP) in SCS's surface sediments and downcore records in the northern SCS were carried out to achieve a quantitative reconstruction of PP and to trace paleoproductivity variations over the last 24 kyr.

2. Oceanographic Settings

The SCS is the largest marginal sea in the western Pacific with an area of 3.5 × 10^6 km^2 [*Wang et al*., 2014] (Figure 1). In the SCS, PP is limited by nutrient availability in the upper water column. Satellite-based annual PP in the northern SCS is about 100–150 g C m^{-2} yr^{-1} with in basin and more than 200 g C m^{-2} yr^{-1} on the continental shelf (Figure 2) [*Behrenfeld and Falkowski*, 1997]. During winter, PP in the northern SCS can be as high as 800 mg C m^{-2} d^{-1} (with a mean value of ~600 mg C m^{-2} d^{-1}), while the mean PP drops to 230 mg C m^{-2} d^{-1} during summer (supporting information Figure S1a) [*Chen*, 2005; *Hao et al*., 2007]. The seasonal variation in PP is mainly driven by the East Asian Monsoon [e.g., *Liu et al*., 2002]. During the winter monsoon prevailing (from November to March), water is well mixed by the surface wind causing the upper photic zone eutrophic and a higher marine PP (supporting information Figures S1a–S1c), which has been proved by both remote and in situ observations [*Liu et al*., 2002; *Chen*, 2005]. In summer monsoon period, hotter and less dense surface water is continually heated and the upper water column turns stratified and oligotrophic. This condition draws a low PP during summer in the northern SCS (supporting information Figures S1a–S1c).

As for the interannual variations, both atmospheric and hydrographic factors play important roles. The winter PP, from December to February, can contribute to more than 40% to the annual PP in the northern SCS (supporting information Figure S1d). Hence, the interannual variations in PP in the northern SCS are mainly caused by the dynamics of winter productivity. The SCS is a semiclosed basin with multiple passages and channels. The major passage between the SCS and the Pacific is the Luzon Strait (Figure 1), through which the Kuroshio Current intrudes into the SCS. The strength of Kuroshio Intrusion is controlled by the El Niño-Southern Oscillation (ENSO) events. [*Nan et al*., 2015]. For example, during El Niño events, more water from western Pacific flows into the SCS making the northern SCS warmer and more oligotrophic [*Qu et al*., 2004; *Caruso et al*., 2006]. El Niño events are accompanied by a weakened EAWM [*Huang et al*., 2004] reducing the upper water mxing. Based on satellite observations, monsoonal influence on mixing plays an important role in the basin and upwelling zones, while PP on the continental shelf has weak correlation with sea surface wind speed (supporting information Figure S3). Hence, both intrusions of oligotrophic water and variations in vertical mixing influence the PP in the northern SCS [e.g., *Voss et al*., 2006; *Liu et al*., 2007; *Zhao and Tang*, 2007; *Ma et al*., 2013]. The winter PP in the northern SCS can diminish by 40–50% (about 30% decrease of annual PP) during a strong El Niño event (supporting information Figure S2).

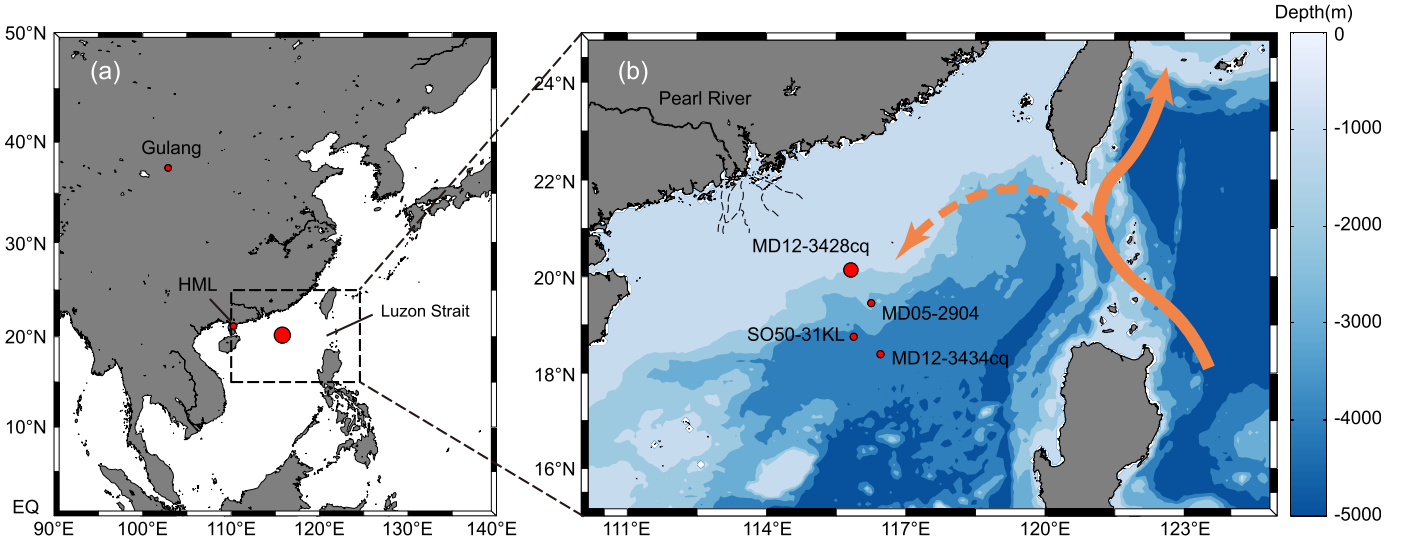

Figure 1. (a) Locations of MD12-3428cq and other sites discussed in the text. The HML means the Huguang Maar Lake. (b) Bathymetry of the study area. Orange solid and dashed lines indicate the Kuroshio Current and Kuroshio Intrusion into the SCS [*Caruso et al*., 2006]. The gray-dashed lines mark the paleo-Pearl River under low sea-level conditions [*Huang et al*., 1995].

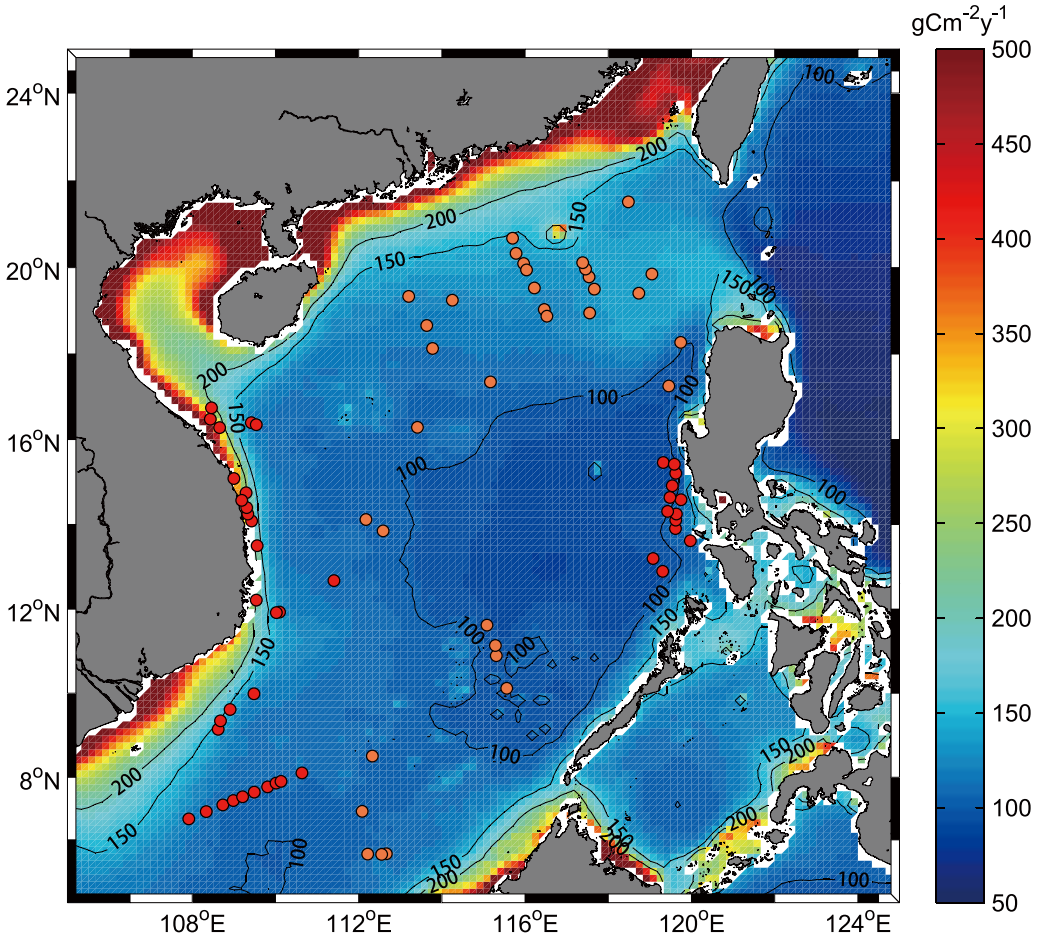

Figure 2. Pattern of 12 year-averaged PP in the SCS from satellite observation. Red and orange circles show the location of the core-top samples used for productivity calibration. The red circles are from *Fernando et al.* [2007] and the orange circles are from the present study.

3. Materials and Methods

3.1. Materials

A sediment core, MD12-3428cq (20°08.48′N; 115°48.8′E; 903 m water depth, Figure 1) was retrieved on the northern SCS continental slope during the "CIRCEA Cruise" [*Kissel et al.*, 2012]. A total of 190 samples from the upper section (3.8 m, total length: 10.15 m) with 2 cm intervals were then prepared for coccolith analyses. In addition, evaluations of %FP from 77 surface sediment and core-top samples were carried out (supporting information Table S1), 34 of which were collected during the R/V Sonne cruises (SO-95) in 1994 [*Sarnthein et al.*, 1994] and subsequently analyzed in the present study. Coccolith data from other samples were acquired from *Fernando et al.* [2007]. Samples deeper than 3500 m (the carbonate compensate depth (CCD) in the SCS) were discarded, as small placoliths are more likely to be dissolved below CCD levels [*Fernando et al.*, 2007].

The 2003–2014 monthly data of PP were obtained from the Ocean Productivity website (http://www.science.oregonstate.edu/ocean.productivity) in hierarchical data format. The conversion of ocean Chl-*a* concentration to PP was based on the vertically generalized production model [*Behrenfeld and Falkowski*, 1997]. In this model, PP is a function of Chl-*a* concentration in surface water, light availability in the water column, and temperature-dependent photosynthetic efficiency. These data were then calculated with MATLAB® to derive a composite 12 year annual average PP with a raw spatial resolution of 0.167°, and then, ultimately interpolated to a resolution of ~3 km (approximately 0.05°).

3.2. Age Model for MD12-3428cq

The age model for the core MD12-3428cq was constructed by accelerator mass spectrometry (AMS) radiocarbon dates, including 15 AMS ^{14}C aging sites of *Globianerinoides ruber* and a linear interpolation between

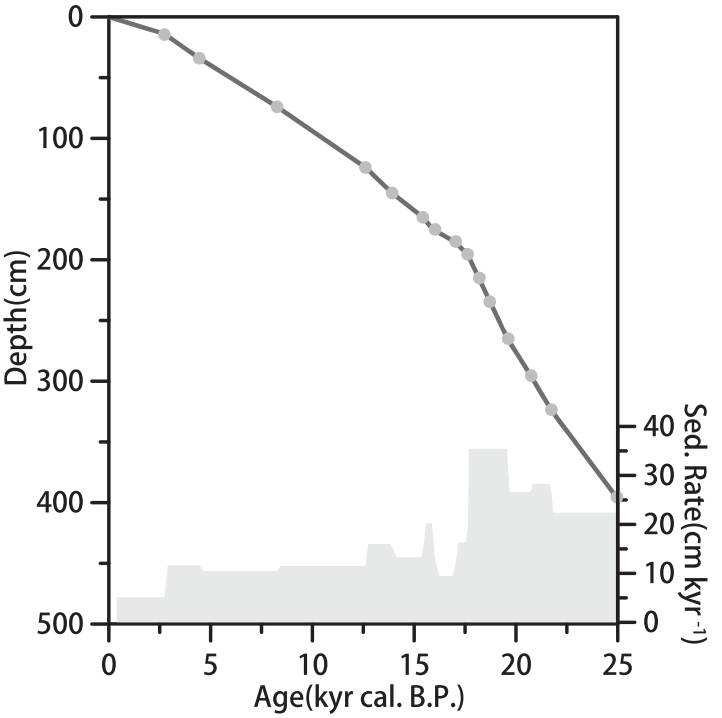

Figure 3. Age model and sedimentation rate for MD12-3428cq. The filled circles represent the planktonic calibration age obtained from *G. ruber*. The shaded area represents the sedimentation rate of MD12-3428cq.

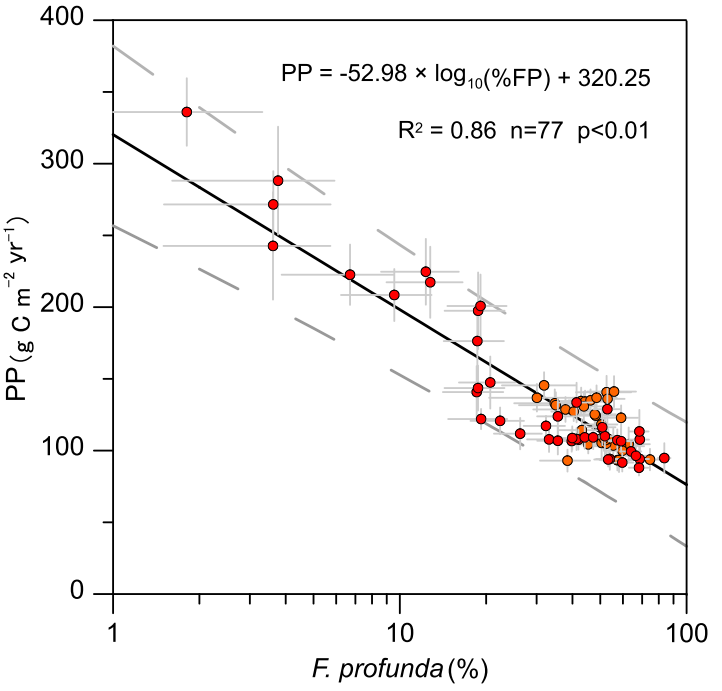

Figure 4. Relationship between %FP in surface samples and modern PP. The red circles are from *Fernando et al.* [2007] and the orange circles are from this study. The gray-dotted lines depict the 95% confidence interval of this study's regressions, which have taken into account the uncertainties of both PP and %FP. The gray error bars represent one standard deviation (1σ) of the satellite-based productivity data and the 66.7% confidence interval of %FP.

them (Figure 3). The samples were measured at the Beta Analytic Laboratory, USA. The CALIB 7.0 program was used to convert AMS ^{14}C ages to calendar years, with a Marine13 radiocarbon calibration curve [*Reimer et al.*, 2013] and a 400 year reservoir correction. The average sedimentation rate of the upper section was determined to be 15.8 cm kyr^{-1} (5.1–35.4 cm kyr^{-1}), equivalent to an average temporal resolution of 126 years (56.4–392 years) for 2 cm sampling intervals (Figure 3).

3.3. Coccolith Analyses

Smear slides were prepared for both downcore and surface sediment samples without performing any chemical pretreatment. Analyses of coccolith assemblages were performed with a polarized light microscope with ×1250 magnification. For each sample, an average of ~1000 (core-top samples) and ~400 (downcore samples) coccolith specimens were counted. %FP were calculated as follow:

$$\%FP = 100 \times (\text{number } F.\ profunda / \text{total coccoliths}) \quad (1)$$

The 95% confidence interval of %FP was calculated following *Patterson and Fishbein's* [1989] method, which depends on the *F. profunda* percentage and the total number of coccoliths counted in each sample (Figure 4).

3.4. Correlation Analyses

Sliding-window correlation analyses were used to assess temporal variations of correlation between the EAWM (grain size, see below) and PP. A window length of 5 kyr was used in our sliding-window correlation analysis because 5 kyr is long enough to insure the significance of results without increasing the "edge effect." More

results of different window length are available in the supporting information (supporting information Figure S4). The cross correlation analyses were applied to detect the potential relationship among records in the Holocene. All analyzed sequences were normalized by Z-score and interpolated into 200 years resolution. For the cross correlation analyses, correlation coefficients on the 0 leg are considered, as the dating uncertainty is less than one lag (200 years) and the PP has a quick response to both EAWM and El Niño [e.g., *Liu et al*., 2002]. All the analyses were performed with the software MATLAB®.

4. Results and Discussions

4.1. %FP Versus PP in the SCS

Among the 77 surface sediment samples in the SCS, %FP varied between 1.8% and 83.6% (N = 77, average = 42.3, $\sigma = 18.6$). A high abundance of *F. profunda* was found in the SCS basin, with a relatively low abundance being found along the Vietnam and Sunda Shelves. The relationship between %FP and modern PP is plotted in Figure 4. To account for PP and %FP data uncertainties, 10,000 regressions were conducted using a Monte Carlo process. The relationship between %FP and PP can be expressed as follows:

$$\mathrm{PP} = -52.98 \times \log_{10}(\%\mathrm{FP}) + 320.25 \quad (2)$$

$$\left(R^2 = 0.86,\ \ \mathrm{n} = 77,\ p < 0.01\right)$$

The exponential inverse-correlation between %FP and PP was first developed and applied by *Beaufort et al*. [1997] for the tropical Indian Ocean and was likewise employed for the Mediterranean Sea [*Incarbona et al*., 2008; *Grelaud et al*., 2012]. Although our formula is quite different from that of previous studies, due to the low PP values of the SCS, the inverse relationship between %FP and PP does appear to be universal in different regions.

4.2. Paleoproductivity in the Northern SCS

The %FP and paleo-PP records in the core MD12-3428cq are shown in Figures 5a and 5b. The %FP of MD12-3428cq vary from 16% to 52% and exhibit millennial variability. The estimated-PP parallels with the %FP record ranging from 110 g C m^{-2} yr^{-1} to 170 g C m^{-2} yr^{-1}. The LGM and early deglacial period are characterized by the highest PP (~170 g C m^{-2} yr^{-1} at 19 and 16 ka), with an average of 158 g C m^{-2} yr^{-1}. From the last deglacial time period to the late Holocene, the estimated PP gradually dropped from ~160 g C m^{-2} yr^{-1} to ~125 g C m^{-2} yr^{-1}. The Holocene experienced the lowest recorded PP, where only 120 g C m^{-2} yr^{-1} are observed.

To detect the reliability of the estimated PP values, nannofloral proxies were compared with geochemical proxies including phytoplankton total biomarkers accumulate rate (PTAR), total biomarker content (PT) [*He et al*., 2013], total organic carbon content (TOC), and organic carbon accumulation rate (OCAR) [*Huang et al*., 1997] (Figures 5c and 5d). The estimated PP, PTAR, and OCAR records in the northern SCS all show remarkable glacial-interglacial variations, with high values in the glacial period and low values in the interglacial period, while the three proxies are quite different in variation magnitudes. The coccolith-based PP decreased by about 23% from 158 g C m^{-2} yr^{-1} in the LGM and early deglacial period to 123 g C m^{-2} yr^{-1} in the Holocene, however, the falls of organic proxies were much sharper during the same interval. PTAR in the core MD05-2904 reached peak at about 19–16 ka with an average value of about 0.19 g m^{-2} kyr^{-1}, while in the Holocene the PTAR dropped to about 0.018 g m^{-2} kyr^{-1} (decreased about 91%). OCAR in the core SO50-31KL reached a maximum during 20–15 ka, where 105.2 mg C cm^{-2} kyr^{-1} was recorded. The Holocene experienced the lowest recorded OCAR, with an average of 31.7 mg C cm^{-2} kyr^{-1} (corresponding to a decrease of about 70%). The difference among productivity records may reflect the variation of organic carbon burial efficiency, which can be defined as ratio of OCAR to estimated-PP. The organic carbon was buried more efficient during the glacial period (about 0.66%, calculated by OCAR/estimated-PP), while the buried efficiency dropped to about 0.26% in the Holocene closed to the modern value [*Zhao et al*., 2009]. The buried efficiency increased with the rise of PP in the northern SCS. However, different patterns were also found in other regions, such as East Pacific [e.g., *Lopes et al*., 2015]. There were evidences that the ventilation of SCS increased in the last deglacial time [*Wan and Jian*, 2014], which may increase the dissolved oxygen in deep water and decrease the organic carbon preservation rate. Hence, the sedimentation rate

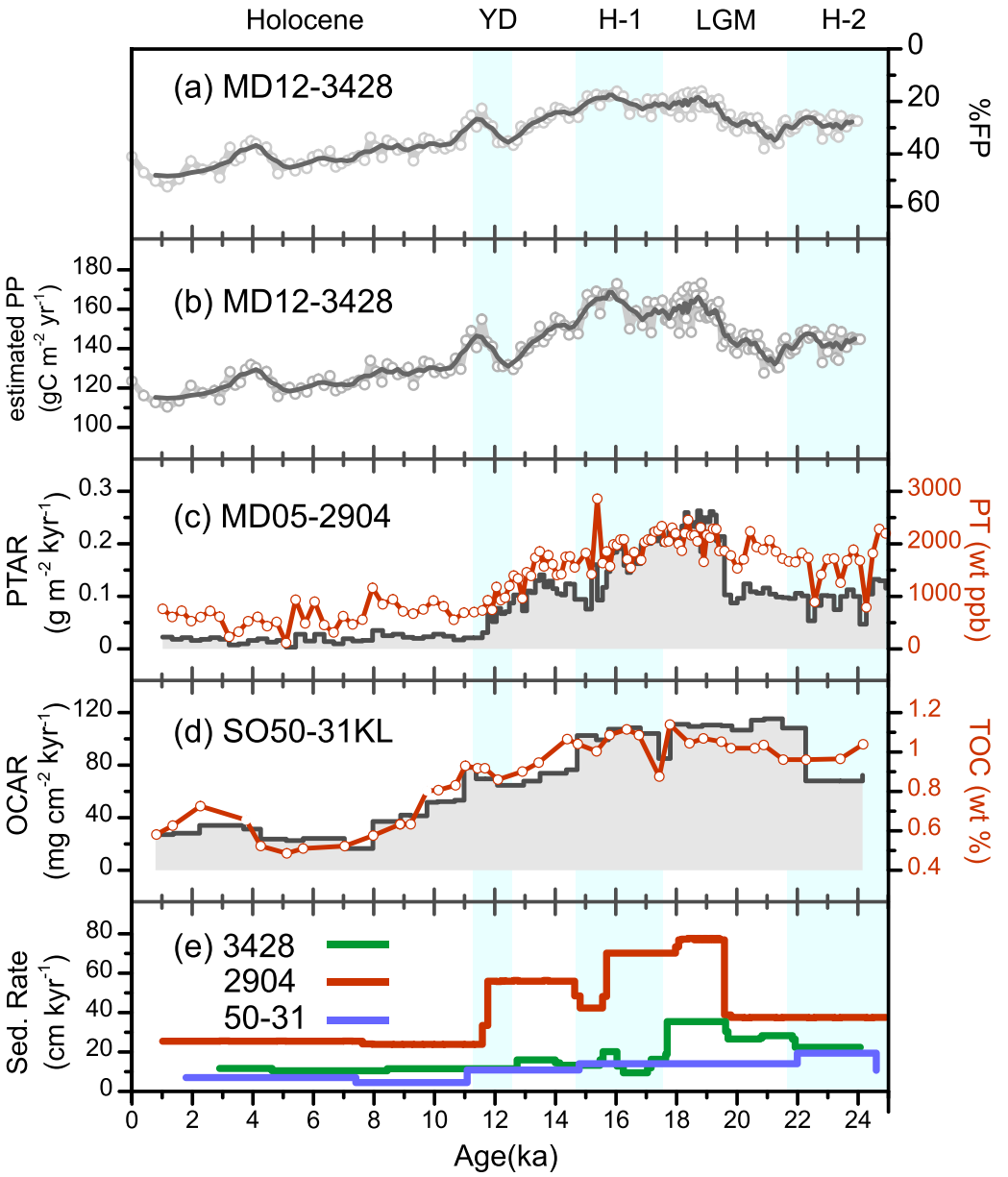

Figure 5. Coccolith assemblages and geochemical proxies in the northern SCS since 25 ka. (a and b) Gray dots represent *F. profunda* percentages (%FP, reverse axis) and (c and d) estimated-PP in MD12-3428cq, with the dark line depicting the weighted average. (c) The phytoplankton total biomarkers accumulation rate (PTAR) and content (PT) in the core MD05-2904 [*He et al.*, 2013] with an improved age model [*Wan and Jian*, 2014]. (d) The organic carbon accumulation rate (OCAR) and total organic carbon content (TOC) in the core SO50-31KL [*Huang et al.*, 1997]. The mass accumulation rate and content data are shown as step plots and line/scatter plots, respectively. (top, e) The sedimentation rates of the three cores presented. Note the different units of estimated PP, PTAR, and OCAR.

may play more important role in the variation of buried efficiency. Since the estimated-PP and the OCAR data are from different cores, more works need to be done before a conclusive result.

4.3. Mechanisms Driving PP in the Northern SCS

To unravel the effect of atmospheric forcing (EAWM) and oceanic forcing (El Niño), we ran a sliding-window correlation analysis and cross correlation analyses between our estimated PP and different paleoenvironment records (Figure 6). The positive correlation between the PP and grain size (used here as a proxy for the EAWM) was strong around 20 ka and from the early deglacial to the early Holocene (Figure 6c). However, this relationship vanished at 7.5 ka. Though the results show a negative correlation around 2.5 ka, this phenomenon cannot be explained by mechanisms described above. If the winter monsoon has any

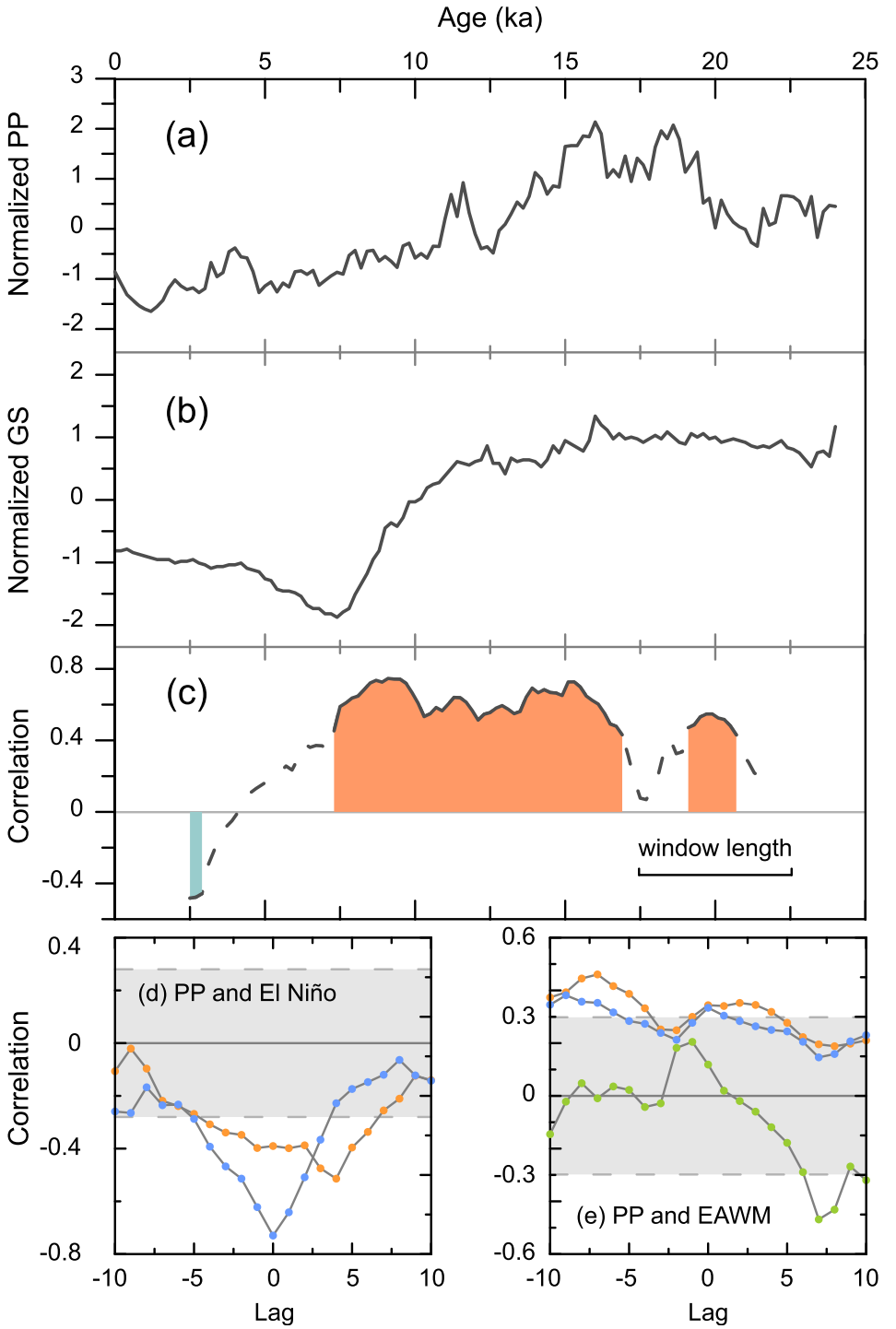

Figure 6. (a) The correlation analysis of the coccolith based PP, EAWM proxies and El Niño. (b) The grain size (GS) stack in northern China loess [*Yang and Ding*, 2014]. (c) Sliding-window correlation analysis was used for PP and GS and (d and e) cross-correlation analysis was used for PP and other environments settings during the Holocene. The shading areas in Figure 6c represent the $p < 0.05$ and the dash lines in Figures 6d and 6e confine the $p = 0.05$ significance threshold. The blue dots in Fieger 6d represent the result of PP and El Niño activity [*Moy et al.*, 2002] and the orange ones represent PP and El Niño strength [*Liu et al.*, 2014a]. Multifold winter monsoon proxies were used in Figure 6e, including the diatom species in Huguang Maar Lake [*Wang et al.*, 2012] (blue dots), surface temperature gradient in the southern SCS [*Huang et al.*, 2011] (orange dots), and surface and subsurface temperature gradient in the northern SCS [*Steinke et al.*, 2011] (green dots). Note the *x* axis of Figures 6d and 6e are Lag (one lag represents 200 years).

correlation with PP, it should be positive correlations. Hence, we infer that the winter monsoon decoupled with PP during this period. The cross correlation analyses between PP and El Niño (including the frequency [*Moy et al*., 2002] and strength [*Liu et al*., 2014a]) show negative correlation between PP and El Niño (Figure 6d), while the EAWM and the estimated PP do not show significant relationship during the Holocene (Figure 6e). Based on our correlation analyses, the PP in the northern SCS decoupled with the strength of EAWM in the Holocene, which means that the winter monsoon controlled productivity hypothesis needs to be improved. Thus, we will explore these possible mechanisms in the flowing.

4.3.1. PP Forced by the EAWM and Sea Level During the LGM and Deglacial

The PP variations in the northern SCS are controlled by many factors, including the monsoon, fluvial inputs, sea level, and other environmental settings [e.g., *Liu et al*., 2002; *Su et al*., 2013]. The higher marine productivity during glacial period can be explained by a strong winter monsoon on glacial-interglacial time scales [e.g., *Huang et al*., 1997; *Higginson et al*., 2003; *Su et al*., 2013]. A strong winter monsoon conventionally enhances water mixing in the northern SCS, thus fueling phytoplankton production in the euphotic zone. Our records have a pattern similar to that of the coccolith-based PP in the Sulu Sea [*Garidel-Thoron et al*., 2001] (Figure 7b), as well as the OCAR and biomarker records in the northern SCS [*Higginson et al*., 2003; *He et al*., 2013], thus confirming the relationship between EAWM and paleoproductivity during the glacial period in the western Pacific marginal seas. As shown in Figure 5b, the estimated PP record presents centennial to millennial scales of oscillations during glacial and deglacial periods. Some oscillations are comparable with the mean grain size of loess in northwestern China [*Sun et al*., 2012; *Yang and Ding*, 2014] (Figures 7c and 7d), especially during the YD and H1, which indicates the strength of EAWM plays an important role in the PP dynamics. The profound sea-level changes during deglaciation altered the terrigenous inputs from the Pearl River to the northern SCS [*Jian et al*., 1999; *Pelejero*, 2003]. The Pearl River delta emerged in low sea level conditions; thus, the distance from the Pearl River estuary to the MD12-3428cq site might be reduced by 40–60% (Figure 1b). The decrease trend in PP from 16 to 13 ka was synchronous with the change in sea level and the associated expected decrease in nutrient loading. However, connections among the estimated-PP, sea level changes, and EAWM in millennial events seem more complex. The strength of winter monsoon during the Heinrich Event 1 (H1) and LGM was almost the same and was a little weaker during the YD [e.g., *Yang and Ding*, 2014]. The PP in H1 was the highest in the last 24 kyr, about 170 g C m^{-2} yr^{-1}, while the PP in LGM and YD were about 150 g C m^{-2} yr^{-1}. That means with a similar winter monsoon and sea level background (Figure 7g), the estimated PP during H1 was about 20 g C m^{-2} yr^{-1} higher than that of LGM. Moreover, the PP in YD was similar to that of LGM though the sea level during the YD was about 60 m higher than that of the LGM.

To interpret the high PP in the H1, the river inputs should be taken into account. *He et al*. [2013] confirmed that odd long chain n-alkane C_{25}-C_{33} in the northern SCS showed covariations with the total phytoplankton biomarkers indicating nutrients from river input also play important role in productivity. *Jian et al*. [2001] noted that the river input was controlled by sea level changes in the glacial-interglacial period. Here we suggested that the precipitation over the South China can also influence the nutrient budget of northern SCS. The summer monsoon was relatively weak during the Younger Dryas (YD) and H1 [e.g., *Wang et al*., 2001]. Based on modeling results, a strong summer monsoon can make more precipitation over the northern China but less over the southern China and vice versa [*Liu et al*., 2014b]. Hence, an increased precipitation associated with a weaker summer monsoon will result in an increase of the Pearl River discharge and then an increase in nutrients loadings. The clay mineral in the northern SCS (MD05-2904) shows the contribution of South China reached maximum at about 17–15ka [*Liu et al*., 2016], which indicating more precipitation in the South China during this period and then causing more nutrients delivered to the northern SCS. The low sea level condition and high precipitation over the South China combined with strong EAWM maximized the PP in the northern SCS. As for the sharp increase of PP during YD, one possible reason is that the EAWM was stronger during this period as suggested by *Huang et al*. [2011]. Another reason is the increased fluvial nutrient inputs. However, the sea level was relatively high, no evidence shows more terrigenous matter deposited during the YD (Figure 7e). Since the strength of winter monsoon cannot be quantitatively reconstructed by proxies so far, it is still hard to separate the influence of monsoon and sea level changes. More works are needed, especially numerical models of marine ecosystems in geological history, to extent the understanding of paleoproductivity.

4.3.2. PP Forced by El Niño During the Holocene

Since only three AMS ^{14}C age constraints were analyzed for the Holocene period of MD12-3428cq, caution is needed in the interpretation of the PP variations during this epoch. Sedimentation rates of different cores

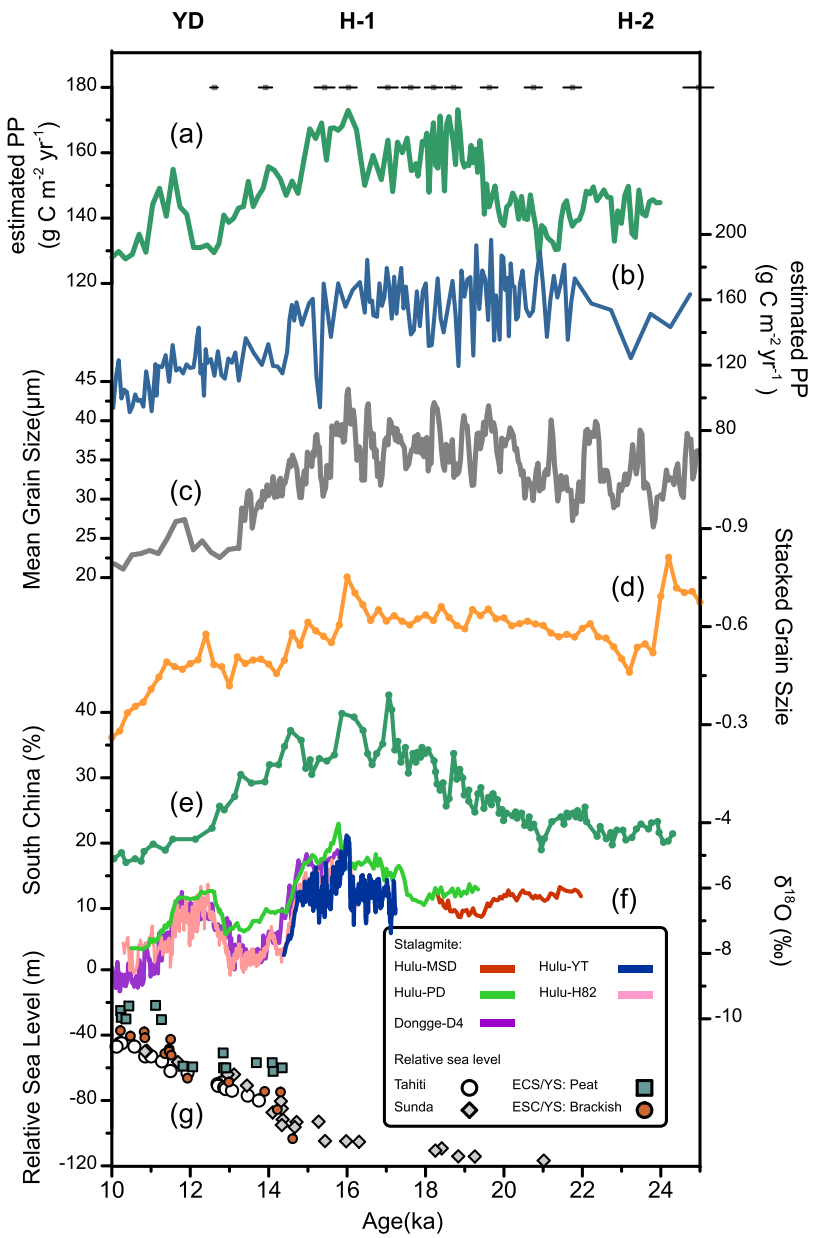

Figure 7. The estimated PP in the (a) northern SCS and (b) the Sulu Sea [*Garidel-Thoron et al*., 2001]. The gray points represent the AMS ^{14}C dating points of MD12-3428cq and the error bars in Figure 7a show the 2σ error for AMS ^{14}C dating. (c) The mean grain size of Gulang loess [*Sun et al*., 2012]. The grain size stack in the northern China loess [*Yang and Ding*, 2014]. The higher values in Figures 7b and 7c and lower value in (d) represent a stronger East Asian Winter Monsoon. (e) South China contribution in clay of the core MD05-2904 [*Liu et al*., 2016]. The δ^{18}O records of Hulu Cave [*Wang et al*., 2001] and Dongge Cave [*Yuan et al*., 2004]. (f) The lower value of δ^{18}O represents a stronger East Asian Summer Monsoon. (g) The Pacific relative sea level in Tahiti [*Bard et al*., 1996; *Montaggioni et al*., 1997], Sunda Shelf [*Lambeck and Chappell*, 2001], and East China Sea (ECS)/Yellow Sea (YS) [*Liu and Milliman*, 2004].

on the upper continental slope seem to remain stable since the middle Holocene [*Huang et al*., 2015]. Therefore, we suggest that the discussions of the Holocene records are reliable. The PP in the northern SCS decreased from the early Holocene to about 5 ka, increased during 5–4.5 ka and was then followed by a decrease trend until 1 ka. Beside the coccolith-based PP, nutrients proxy Cd/Ca ratio of *G. ruber*, in the core MD12-3434cq shows a similar pattern during the Holocene (X. Wang and Z. Jian, unpublished data, 2016, Figure 8b). Recent studies from high-resolution marine and lacustrine sedimentation have suggested that EAWM had a sharp decrease in 6 ka followed by a relatively stable stage or a gently increase until the late Holocene [e.g., *Huang et al*., 2011; *Steinke et al*., 2011; *Wang et al*., 2012; *Jia et al*., 2015] (Figures 8d–8f). The

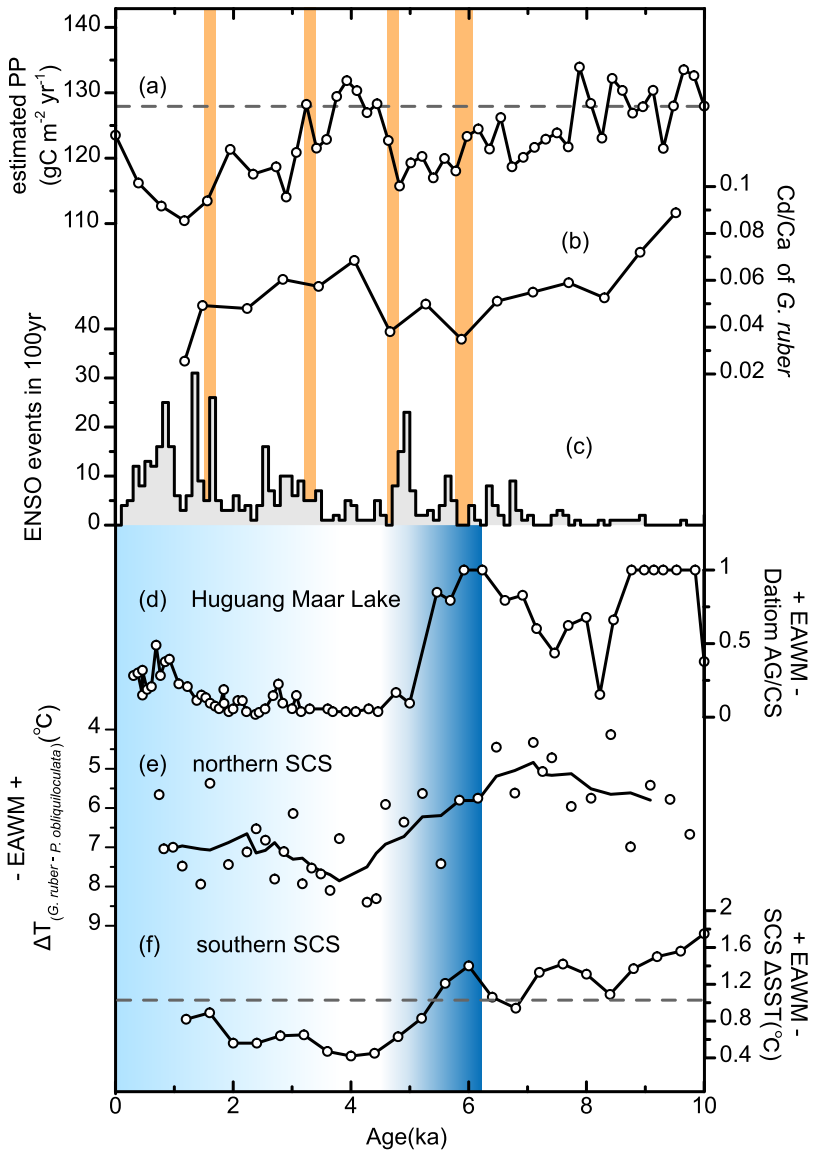

Figure 8. The PP in the northern SCS and other paleoclimate records of the Holocene period. (a) The coccolith-based PP in the northern SCS. The gray-dashed line represents the modern PP at the site of MD12-3428cq (128 g C m^{-2} yr^{-1}). (b) The Cd/Ca ratio of *G. ruber* in the core MD12-3434cq (Wang and Jian, unpublished data). (c) The number of El Niño events per 100 years in the Laguna Pallcacocha of South America [*Moy et al.*, 2002]. The orange-shading areas represent the sedimentary events recognized in the northeastern SCS which was caused by the Kuroshio Intrusion [*Liu et al.*, 2013]. (d) The ratio of two diatom species *Aulacoseira granulate* to *Cyclotella stelligera* in the Huguang Maar Lake of China [*Wang et al.*, 2012]. (e) The temperature gradient between *G. ruber* and *P. obliquiloculata* in the core MD05-2904 [*Steinke et al.*, 2011]. (f) The SST gradient between the southwestern and southeastern SCS [*Huang et al.*, 2011]. The gray-dashed line represents the modern gradient (1°C). Higher values in Figures 8d and 8f and lower values in Figure 8e represent a stronger East Asian Winter Monsoon (EAWM).

PP variation was quite different from EAWM pattern during the Holocene, which can be illustrated by correlation analyses (Figure 6e).

Water structure can be reconstructed by temperature gradient between the surface water (Mg/Ca of *G. ruber*) and subsurface water (Mg/Ca of *Pulleniatina obliquiloculata*), which represents the winter monsoon controlled water mixing [*Steinke et al.*, 2010]. A stronger winter monsoon causes a stronger mixing, more homogeneous water, a smaller temperature gradient and a deeper thermocline, hence the temperature gradient (ΔT) in the northern SCS shows that the water structure was controlled by the winter monsoon. The ΔT in core MD05-2904 shows similar pattern with other EAWM proxies around the SCS with decreasing trend in about 6 ka and then increasing in the late Holocene (Figure 8e) [*Steinke et al.*, 2011]. The different

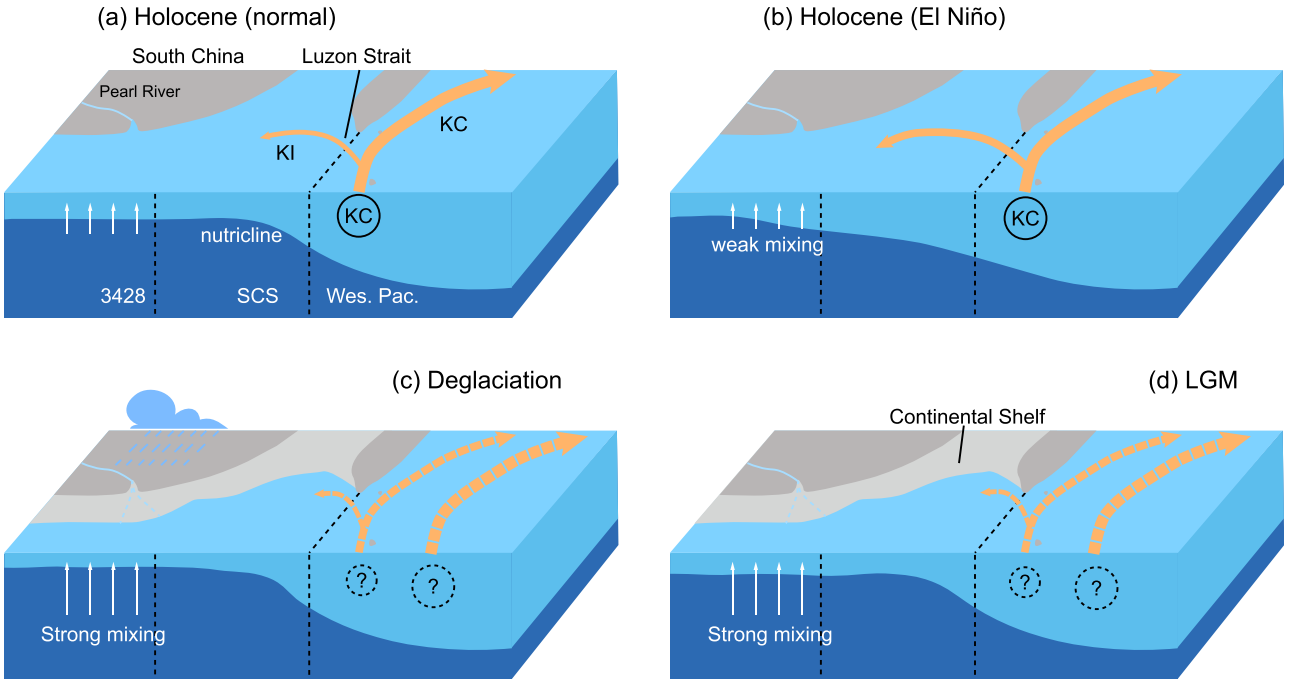

Figure 9. Conceptual model of the paleoceanographic changes related to the dynamics of PP in the northern SCS. The light and dark-blue segments represent low-nutrient water and high-nutrient water, respectively. The white arrows represent wind-driven water mixing, which was weaker in the Holocene and stronger during the deglaciation and LGM. "KI" means Kuroshio Intrusion into the SCS and "KC" means the Kuroshio Current in the western Pacific. (a) During the Holocene non-El Niño years, the Kuroshio only intruded into the northeastern SCS resulting in a shallow nutricline and a high PP in the northern SCS. (b) In the Holocene El Niño years, the Kuroshio Intrusion into the northern SCS (along with a weakened mixing) led to a deep nutricline level and a low PP. In the LGM and the last deglaciation, the Kuroshio might have moved eastward (or altogether weakened), variations of EAWM, sea level, and rainfall control the PP in the northern SCS.

patterns of water structure (ΔT) and marine productivity (%FP, OCAR and Cd/Ca ratio) in the northern SCS (Figures 5 and 8) indicate that the vertical mixing decoupled with nutrient concentration of the upper water column. Variations in PP generally followed the pattern of El Niño event in the Holocene showing a strong negative correlation (Figure 6). We proposed that the main controlling factor of PP changed from EAWM to El Niño since the mid-Holocene period, as El Niño events occurred more frequently and stronger.

According to modern oceanographic observations, the Kuroshio Current is seen to weaken during El Niño events and intrudes into the northern SCS area more intensely [*Qu et al.*, 2004; *Caruso et al.*, 2006]. This event typically brings oligotrophic western Pacific water into the northern SCS and changes the nutrient distribution of the upper water column accordingly. Paleoclimate records and model studies suggest that a gradual intensification of El Niño has occurred over the past 6 kyr [e.g., *Moy et al.*, 2002; *Liu et al.*, 2014a]. A strong El Niño event can cause a reduction of annual PP by 30–40% (supporting information Figure S2), i.e., about 40–50 g C m^{-2} y^{-1} with regard to the early Holocene level (~130 g C m^{-2} y^{-1}). Therefore, if 30 El Niño events had occurred in a 100 years span, assuming the strength of El Niño was stable, this would lead to a reduction of 100 year-averaged PP to 116.35 g C m^{-2} y^{-1}, which can be calculated as follow:

$$\text{Averaged PP} = (70\times130+30\times0.65\times130)/100 = 116.35 \text{ g C } m^{-2}yr^{-1}$$

This estimation is closed to our downcore result (about 110 g C m^{-2} yr^{-1}). We also notice that the correlation between PP and the frequency of El Niño is more significant than that between PP and strength of El Niño (Figure 6d). We suggest that the frequency plays more important roles on PP in the northern SCS. When the western Pacific water flows into the northern SCS, PP decreases sharply. However, a stronger El Niño event cannot make the water more oligotrophic or further decrease the PP. Hence, the frequency of El Niño becomes the key factor nor the strength of El Niño. To conclude, the decrease in PP during 8–5 ka and 4–1 ka was caused by strong Kuroshio Intrusions into the SCS. The enhanced Kuroshio Intrusion scenario offers an explanation to why productivity in the northern SCS decreased without any significant EAWM changes during these periods. This interpretation was also supported by the sediment records from northeastern SCS, which indicated that four stronger Kuroshio Intrusion events occurred during the Holocene

(Figure 8) [*Liu et al*., 2013]. While during low sea-level conditions, the Kuroshio Current notably decreased and its main stream ultimately moved eastward [*Ujiié et al*., 2003; *Kao et al*., 2006]. It is therefore suggested that PP in the northern SCS received less impact from the Kuroshio Current during the LGM and the last deglaciation period (Figures 9c and 9d).

5. Conclusions

By analyzing the relationship between %FP in surface sedimentation and PP, a new PP transfer formula in the SCS was successfully obtained. Based on this formula, paleoproductivity was reconstructed in the northern SCS over the last 24 kyr. The PP variations have a significant glacial-deglacial pattern, while the magnitude of variation was much smaller than the organic proxies indicating that organic carbon burial efficiency varied in the SCS. Correlation analyses results indicated that the main controlling factors of PP in the northern SCS shifted from EAWM to El Niño during the mid-Holocene period. During the early deglacial period and LGM, with a background of strong EAWM and low sea level condition, PP varied with EAWM oscillations and was also influenced by rainfall over the South China. The rapid increase in sea level and dramatic decrease in EAWM intensities resultantly reduced nutrient supplies to upper water, which ultimately dropped PP values from ~170 g C m^{-2} yr^{-1} during the LGM and H1 to ~120 g C m^{-2} yr^{-1} during the early Holocene. Since the mid-Holocene, the gradual increase in both frequency and strength of El Niño events strengthened the Kuroshio Intrusion into the northern SCS and oligotrophic western Pacific water from the Kuroshio Current reduced the PP in the northern SCS.

Acknowledgments

We thank the French Polar Institute (IPEV) for their technique in retrieving samples during the MD-190 CIRCEA cruise in 2012. We appreciate Xing-Xing Wang for providing Cd/Ca ratio data, Meng Wang, Huangmin Ge, and Iván Hernández-Almeida for their insightful discussions. We thank two anonymous reviewers for their valuable suggestions. This study was supported by the National Science Foundation of China (grant 91228204 and 41376047). The %FP data are available in the supporting information Tables S1 and S2 in the SI file and any additional data may be obtained from H. Zhang (email: 103443_rui@tongji.edu.cn).

References

Bard, E., B. Hamelin, M. Arnold, L. Montaggioni, G. Cabioch, G. Faure, and F. Rougerie (1996), Deglacial sea-level record from Tahiti corals and the timing of global meltwater discharge, *Nature*, *382*(6588), 241–244, doi:10.1038/382241a0.

Beaufort, L., Y. Lancelot, P. Camberlin, O. Cayre, E. Vincent, F. Bassinot, and L. Labeyrie (1997), Insolation cycles as a major control of equatorial Indian Ocean primary production, *Science*, *278*(5342), 1451–1454, doi:10.1126/science.278.5342.1451.

Beaufort, L., T. de Garidel-Thoron, A. C. Mix, and N. G. Pisias (2001), ENSO-like forcing on oceanic primary production during the late Pleistocene, *Science*, *293*(5539), 2440–2444, doi:10.1126/science.293.5539.2440.

Behrenfeld, M. J., and P. G. Falkowski (1997), Photosynthetic rates derived from satellite-based chlorophyll concentration, *Limnol. Oceanogr.*, *42*(1), 1–20, doi:10.4319/lo.1997.42.1.0001.

Caruso, M. J., G. G. Gawarkiewicz, and R. C. Beardsley (2006), Interannual variability of the Kuroshio intrusion in the South China Sea, *J. Oceanogr.*, *62*(4), 559–575.

Chen, Y.-l. L. (2005), Spatial and seasonal variations of nitrate-based new production and primary production in the South China Sea, *Deep Sea Res., Part I*, *52*(2), 319–340, doi:10.4067/s0717-65382004000200017.

Fernando, A. G. S., A. M. Peleo-Alampay, and M. G. Wiesner (2007), Calcareous nannofossils in surface sediments of the eastern and western South China Sea, *Mar. Micropaleontol.*, *66*(1), 1–26, doi:10.1016/j.marmicro.2007.07.003,

Garidel-Thoron, T., L. Beaufort, B. K. Linsley, and S. Dannenmann (2001), Millennial-scale dynamics of the east Asian winter monsoon during the last 200,000 years, *Paleoceanography*, *16*(5), 491–502, doi:10.1029/2000pa000557.

Giraudeau, J., and L. Beaufort (2007), Coccolithophores: From extant populations to fossil assemblages, in *Proxies in Late Cenozoic Paleoceanography*, Dev. in Mar. Geol., vol. 1, edited by C. Hillaire-Marcel and A. de Vernal, pp. 409–439, Elsevier, Amsterdam, doi:10.1016/s1572-5480(07)01015-9.

Grelaud, M., G. Marino, P. Ziveri, and E. J. Rohling (2012), Abrupt shoaling of the nutricline in response to massive freshwater flooding at the onset of the last interglacial sapropel event, *Paleoceanography*, *27*, PA3208, doi:10.1029/2012PA002288.

Hao, Q., X. Ning, C. Liu, Y. Cai, and F. Le (2007), Satellite and in situ observations of primary production in the northern South China Sea 336 [in Chinese with English abstract], *Acta Oceanol. Sin.*, *3*, 58–67.

He, J., M. Zhao, P. Wang, L. Li, and Q. Li (2013), Changes in phytoplankton productivity and community structure in the northern South China Sea during the past 260ka, *Palaeogeogr. Palaeoclimatol. Palaeoecol.*, *392*, 312–323, doi:10.1016/j.palaeo.2013.09.010.

Higginson, M. J., J. R. Maxwell, and M. A. Altabet (2003), Nitrogen isotope and chlorin paleoproductivity records from the Northern South China Sea: Remote vs. local forcing of millennial-and orbital-scale variability, *Mar. Geol.*, *201*(1), 223–250, doi:10.1016/s0025-3227(03)00218-4.

Huang, C.-Y., P.-M. Liew, M. Zhao, T.-C. Chang, C.-M. Kuo, M.-T. Chen, C.-H. Wang, and L.-F. Zheng (1997), Deep sea and lake records of the Southeast Asian paleomonsoons for the last 25 thousand years, *Earth Planet. Sci. Lett.*, *146*(1), 59–72, doi:10.1016/s0012-821x(96)00203-8.

Huang, E., J. Tian, and S. Steinke (2011), Millennial-scale dynamics of the winter cold tongue in the southern South China Sea over the past 26ka and the East Asian winter monsoon, *Quat. Res.*, *75*(1), 196–204, doi:10.1016/j.yqres.2010.08.014.

Huang, E., J. Tian, P. Qiao, S. Wan, X. Xie, and W. Yang (2015), Early interglacial carbonate-dilution events in the South China Sea: Implications for strengthened typhoon activities over subtropical East Asia, *Quat. Sci. Rev.*, *125*, 61–77, doi:10.1016/j.quascirev.2015.08.007.

Huang, R., W. Chen, B. Yang, and R. Zhang (2004), Recent advances in studies of the interaction between the East Asian winter and summer monsoons and ENSO cycle, *Adv. Atmos. Sci.*, *21*(3), 407–424, doi:10.1007/bf02915568.

Huang, Z., W. Zhang, and F. Cai (1995), The submerged Pearl River delta [in Chinese with English abstract], *Acta Geogr. Sin.*, *50*(3), 206–214.

Incarbona, A., E. Di Stefano, B. Patti, N. Pelosi, S. Bonomo, S. Mazzola, R. Sprovieri, G. Tranchida, S. Zgozi, and A. Bonanno (2008), Holocene millennial-scale productivity variations in the Sicily Channel (Mediterranean Sea), *Paleoceanography*, *23*, PA3204, doi:10.1029/2007PA001581.

Jia, G., Y. Bai, X. Yang, L. Xie, G. Wei, T. Ouyang, G. Chu, Z. Liu, and P. A. Peng (2015), Biogeochemical evidence of Holocene East Asian summer and winter monsoon variability from a tropical maar lake in southern China, *Quat. Sci. Rev.*, *111*, 51–61, doi:10.1016/j.quascirev.2015.01.002.

Jian, Z., L. Wang, M. Kienast, M. Sarnthein, W. Kuhnt, H. Lin, and P. Wang (1999), Benthic foraminiferal paleoceanography of the South China Sea over the last 40,000 years, *Mar. Geol.*, *156*(1), 159–186, doi:10.1016/s0025-3227(98)00177-7.

Jian, Z., B. Huang, W. Kuhnt, and H.-L. Lin (2001), Late Quaternary upwelling intensity and East Asian monsoon forcing in the South China Sea, *Quat. Res.*, *55*(3), 363–370, doi:10.1006/qres.2001.2231.

Jin, X., C. Liu, A. J. Poulton, M. Dai, and X. Guo (2016), Coccolithophore responses to environmental variability in the South China Sea: Species composition and calcite content, *Biogeosciences*, *13*(16), 4843–4861, doi:10.5194/bg-13-4843-2016.

Kao, S. J., C. R. Wu, Y. C. Hsin, and M. Dai (2006), Effects of sea level change on the upstream Kuroshio Current through the Okinawa Trough, *Geophys. Res. Lett.*, *33*, L16604, doi:10.1029/2006GL026822.

Kissel, C., Z. Jian, and the Shipboard Scientific Party (2012), MD190-CIRCEA Cruise Report, ref: OCE/2012/01, Institut polaire français - Paul Emile Victor (IPEV), Brest.

Lambeck, K., and J. Chappell (2001), Sea level change through the last glacial cycle, *Science*, *292*(5517), 679–686, doi:10.1126/science.1059549.

Lin, H.-L., C.-T. Lai, H.-C. Ting, L. Wang, M. Sarnthein, and J.-J. Hung (1999), Late Pleistocene nutrients and sea surface productivity in the South China Sea: A record of teleconnections with Northern Hemisphere events, *Mar. Geol.*, *156*(1), 197–210, doi:10.1016/s0025-3227(98)00179-0.

Liu, C., P. Wang, J. Tian, and X. Cheng (2008), Coccolith evidence for Quaternary nutricline variations in the southern South China Sea, *Mar. Micropaleontol.*, *69*(1), 42–51, doi:10.1016/j.marmicro.2007.11.008.

Liu, H., J. Chang, C.-M. Tseng, L.-S. Wen, and K. Liu (2007), Seasonal variability of picoplankton in the Northern South China Sea at the SEATS station, *Deep Sea Res., Part II*, *54*(14), 1602–1616, doi:10.1016/j.dsr2.2007.05.004.

Liu, J., T. Li, R. Xiang, M. Chen, W. Yan, Z. Chen, and F. Liu (2013), Influence of the Kuroshio Current intrusion on Holocene environmental transformation in the South China Sea, *Holocene*, *23*(6), 850–859, doi:10.1177/0959683612474481.

Liu, J. P., and J. D. Milliman (2004), Reconsidering melt-water pulses 1A and 1B: Global impacts of rapid sea-level rise, *J. Ocean Univ. China*, *3*(2), 183–190, doi:10.1007/s11802-004-0033-8.

Liu, K.-K., S.-Y. Chao, P.-T. Shaw, G.-C. Gong, C.-C. Chen, and T. Tang (2002), Monsoon-forced chlorophyll distribution and primary production in the South China Sea: Observations and a numerical study, *Deep Sea Res., Part I*, *49*(8), 1387–1412, doi:10.1016/s0967-0637(02)00035-3.

Liu, Z., Z. Lu, X. Wen, B. Otto-Bliesner, A. Timmermann, and K. Cobb (2014a), Evolution and forcing mechanisms of El Niño over the past 21,000 years, *Nature*, *515*(7528), 550–553, doi:10.1038/nature13963.

Liu, Z., et al. (2014b), Chinese cave records and the East Asia Summer Monsoon, *Quat. Sci. Rev.*, *83*, 115–128, doi:10.1016/j.quascirev.2013.10.021.

Liu, Z., et al. (2016), Source-to-sink transport processes of fluvial sediments in the South China Sea, *Earth Sci. Rev.*, *153*, 238–273, doi:10.1016/j.earscirev.2015.08.005.

Lopes, C., M. Kucera, and A. C. Mix (2015), Climate change decouples oceanic primary and export productivity and organic carbon burial, *Proc. Natl. Acad. Sci. U. S. A.*, *112*(2), 332–335, doi:10.1073/pnas.1410480111.

Löwemark, L., S. Steinke, C. H. Wang, M. T. Chen, A. Müller, L. J. Shiau, S. J. Kao, S. R. Song, H. L. Lin, and K. Y. Wei (2009), New evidence for a glacioeustatic influence on deep water circulation, bottom water ventilation and primary productivity in the South China Sea, *Dyn. Atmos. Oceans*, *47*(1–3), 138–153, doi:10.1016/j.dynatmoce.2008.08.004.

Ma, W., F. Chai, P. Xiu, H. Xue, and J. Tian (2013), Modeling the long-term variability of phytoplankton functional groups and primary productivity in the South China Sea, *J. Oceanogr.*, *69*(5), 527–544, doi:10.1007/s10872-013-0190-8.

Martin, J. H. (1990), Glacial-interglacial CO2 change: The iron hypothesis, *Paleoceanography*, *5*(1), 1–13, doi:10.1029/pa005i001p00001.

Molfino, B., and A. McIntyre (1990), Precessional forcing of nutricline dynamics in the Equatorial Atlantic, *Science*, *249*(4970), 766–769, doi:10.1126/science.249.4970.766.

Montaggioni, L. F., G. Cabioch, G. F. Camoin, E. Bard, A. R. Laurenti, G. Faure, P. Déjardin, and J. Récy (1997), Continuous record of reef growth over the past 14 ky on the mid-Pacific island of Tahiti, *Geology*, *25*(6), 555–558, doi:10.1130/0091-7613(1998)026<0479:CRORGO>2.3.CO;2.

Moy, C. M., G. O. Seltzer, D. T. Rodbell, and D. M. Anderson (2002), Variability of El Niño/Southern Oscillation activity at millennial timescales during the Holocene epoch, *Nature*, *420*(6912), 162–165, doi:10.1038/nature01194.

Nan, F., H. Xue, and F. Yu (2015), Kuroshio intrusion into the South China Sea: A review, *Prog. Oceanogr.*, *137*, 314–333, doi:10.1016/j.pocean.2014.05.012.

Patterson, R. T., and E. Fishbein (1989), Re-examination of the statistical methods used to determine the number of point counts needed for micropaleontological quantitative research, *J. Paleontol.*, *63*(2), 245–248, doi:10.1017/s0022336000019272.

Pelejero, C. (2003), Terrigenous n-alkane input in the South China Sea: High-resolution records and surface sediments, *Chem. Geol.*, *200*(1), 89–103, doi:10.1016/s0009-2541(03)00164-5.

Poulton, A. J., A. Charalampopoulou, J. R. Young, G. A. Tarran, M. I. Lucas, and G. D. Quartlya (2010), Coccolithophore dynamics in nonbloom conditions during late summer in the central Iceland Basin (July-August 2007), *Limnol. Oceanogr.*, *55*(4), 1601–1613, doi:10.4319/lo.2010.55.4.1601.

Qu, T., Y. Y. Kim, M. Yaremchuk, T. Tozuka, A. Ishida, and T. Yamagata (2004), Can Luzon Strait transport play a role in conveying the impact of ENSO to the South China Sea?, *J. Clim.*, *17*(18), 3644–3657, doi:10.1175/1520-0442(2004)017<3644:CLSTPA>2.0.CO;2.

Reimer, P. J., E. Bard, A. Bayliss, J. W. Beck, P. G. Blackwell, C. Bronk Ramsey, C. E. Buck, H. Cheng, R. L. Edwards, and M. Friedrich (2013), IntCal13 and Marine13 radiocarbon age calibration curves 0-50,000 years cal BP, *Radiocarbon*, *55*(4), 1869–1887, doi:10.2458/azu_js_rc.55.16947.

Sarnthein, M., U. Pflaumann, P. Wang, and H. Wong (1994), Preliminary report on Sonne-95 cruise "monitor monsoon" to the South China Sea, Berich-Report, *Geol.-Palaont. Insttitut der Universität Kiel*, *68*, 1–225.

Sprengel, C., K.-H. Baumann, J. Henderiks, R. Henrich, and S. Neuer (2002), Modern coccolithophore and carbonate sedimentation along a productivity gradient in the Canary Islands region: Seasonal export production and surface accumulation rates, *Deep Sea Res., Part II*, *49*(17), 3577–3598, doi:10.1016/s0967-0645(02)00099-1.

Steinke, S., M. Mohtadi, J. Groeneveld, L.-C. Lin, L. Löwemark, M.-T. Chen, and R. Rendle-Bühring (2010), Reconstructing the southern South China Sea upper water column structure since the Last Glacial Maximum: Implications for the East Asian winter monsoon development, *Paleoceanography*, *25*, PA2219, doi:10.1029/2009PA001850.

Steinke, S., C. Glatz, M. Mohtadi, J. Groeneveld, Q. Li, and Z. Jian (2011), Past dynamics of the East Asian monsoon: No inverse behaviour between the summer and winter monsoon during the Holocene, *Global Planet. Change*, *78*(3–4), 170–177, doi:10.1016/j.gloplacha.2011.06.006.

Su, X., C. Liu, L. Beaufort, J. Tian, and E. Huang (2013), Late Quaternary coccolith records in the South China Sea and East Asian monsoon dynamics, *Global Planet. Change*, *111*, 88–96, doi:10.1016/j.gloplacha.2013.08.016.

Sun, Y., S. C. Clemens, C. Morrill, X. Lin, X. Wang, and Z. An (2012), Influence of Atlantic meridional overturning circulation on the East Asian winter monsoon, *Nat. Geosci.*, *5*(1), 46–49, doi:10.1038/ngeo1326.

Ujiié, Y., H. Ujiié, A. Taira, T. Nakamura, and K. Oguri (2003), Spatial and temporal variability of surface water in the Kuroshio source region, Pacific Ocean, over the past 21,000 years: Evidence from planktonic foraminifera, *Mar. Micropaleontol.*, *49*(4), 335–364, doi:10.1016/s0377-8398(03)00062-8.

Voss, M., D. Bombar, N. Loick, and J. W. Dippner (2006), Riverine influence on nitrogen fixation in the upwelling region off Vietnam, South China Sea, *Geophys. Res. Lett.*, *33*, L07604, doi:10.1029/2005GL025569.

Wan, S., and Z. Jian (2014), Deep water exchanges between the South China Sea and the Pacific since the last glacial period, *Paleoceanography*, *29*, 1162–1178, doi:10.1002/2013PA002578.

Wang, L., et al. (2012), The East Asian winter monsoon over the last 15,000 years: Its links to high-latitudes and tropical climate systems and complex correlation to the summer monsoon, *Quat. Sci. Rev.*, *32*, 131–142, doi:10.1016/j.quascirev.2011.11.003.

Wang, P., Q. Li, and C.-F. Li (2014), *Geology of the China Seas*, Elsevier, Amsterdam, doi:10.1016/c2011-0-00049-2.

Wang, R., Z. Jian, W. Xiao, J. Tian, J. Li, R. Chen, Y. Zheng, and J. Chen (2007), Quaternary biogenic opal records in the South China Sea: Linkages to East Asian monsoon, global ice volume and orbital forcing, *Sci. China Ser. D*, *50*(5), 710–724, doi:10.1007/s11430-007-0041-9.

Wang, Y. J., H. Cheng, R. L. Edwards, Z. S. An, J. Y. Wu, C.-C. Shen, and J. A. Dorale (2001), A High-Resolution Absolute-Dated Late Pleistocene Monsoon Record from Hulu Cave, China, *Science*, *294*(5550), 2345–2348, doi:10.1126/science.1064618.

Wei, G., Y. Liu, X. Li, M. Chen, and W. Wei (2003), High-resolution elemental records from the South China Sea and their paleoproductivity implications, *Paleoceanography*, *18*(2), 1054, doi:10.1029/2002PA000826.

Yang, S., and Z. Ding (2014), A 249 kyr stack of eight loess grain size records from northern China documenting millennial-scale climate variability, *Geochem. Geophys. Geosyst.*, *15*, 798–814, doi:10.1002/2013gc005113.

Young, J. R., and P. Ziveri (2000), Calculation of coccolith volume and it use in calibration of carbonate flux estimates, *Deep Sea Res., Part II*, *47*(9), 1679–1700, doi:10.1016/s0967-0645(00)00003-5.

Yuan, D., et al. (2004), Timing, duration, and transitions of the last interglacial Asian monsoon, *Science*, *304*(5670), 575–578, doi:10.1126/science.1091220.

Zhao, H., and D. L. Tang (2007), Effect of 1998 El Niño on the distribution of phytoplankton in the South China Sea, *J. Geophys. Res.*, *112*, C02017, doi:10.1029/2006JC003536.

Zhao, M., C.-Y. Huang, C.-C. Wang, and G. Wei (2006), A millennial-scale U 37 K′ sea-surface temperature record from the South China Sea (8 N) over the last 150 kyr: Monsoon and sea-level influence, *Palaeogeogr. Palaeoclimatol. Palaeoecol.*, *236*(1), 39–55, doi:10.1016/j.palaeo.2005.11.033.

Zhao, M., P. Wang, J. Tian, and J. Li (2009), Biogeochemistry and the carbon reservoir, in *The South China Sea*, Dev. Paleoenvironment. Res., vol.13, edited by P. Wang and Li Q., pp. 439–483, Springer, Amsterdam, doi:10.1007/978-1-4020-9745-4_7.